

A study on the classification performance of water-injection hydrocyclone

Peikun Liu¹, Zhongzhi Gao¹, Xinghua Yang¹, Duanxu Hou¹, Lanyue Jiang¹, Zhihua Jiang², Zhongxi Yan²

¹ College of Mechanical and Electronic Engineering, Shandong University of Science and Technology, Qingdao 266590, China

² Dandong Dongfang Measurement & Control Technology Co., Ltd, Dandong 118002, China

Corresponding author: skd992489@sdust.edu.cn (Xinghua Yang)

Abstract: Aiming at the problem of fine particles entrainment in the underflow of hydrocyclone during the metal grinding classification process, a water-injection hydrocyclone was proposed to improve the classification efficiency. Through external injection of water on the wall surface of the cone section, the particles settling in the region were loosely graded so that the fine particles settled in the wall surface returned to the inner swirl again, thus reducing their entry into the underflow. Numerical simulation was used to explore the differences in the internal flow field characteristics and separation performance of the hydrocyclone after adding the water-injection structure. Then the industrial tests were conducted on the classification performance of the water-injection hydrocyclone. Numerical results showed that compared with the conventional hydrocyclone, the static pressure, tangential and axial velocity of the fluid inside the water-injection hydrocyclone increased, while the turbulence intensity decreased. The experimental results showed that with the increase of water-injection flow rate, the content of -74 μm particles in the underflow of water-injection hydrocyclone first decreased and then increased, and the comprehensive classification efficiency increased and then decreased accordingly. Compared with the conventional hydrocyclone, the content of -74 μm particles in the underflow of the water-injection hydrocyclone was reduced from 26.34% to 23.95%, and the comprehensive classification efficiency was increased from 69.22% to 73.03%, which mitigated the phenomenon of fine particles entrainment in the underflow.

Keywords: water-injection hydrocyclone, numerical simulation, industrial tests, classification performance

1. Introduction

Hydrocyclone is a kind of equipment that utilizes centrifugal force and gravity for classification, with a simple structure, small footprint, low operating cost, and high separation efficiency. Therefore, hydrocyclone was widely used in metal ore grinding and classifying operations (Mognon et al., 2015; Dehdarnejad and Bayareh, 2021; Wang et al., 2019; Zhang et al., 2023). Conventional hydrocyclone was prone to remixing the separated fine particles into the underflow due to the disturbance of the flow field near the underflow during the classification process. At the same time, due to the gradual increase of particle concentration in the lower cone section of the hydrocyclone and the small separation space, some of the fine particles were sucked into the underflow by the coarse particles, resulting in the underflow of the hydrocyclone to clip the fine particles, which reduces the grading accuracy (Ghodrat et al., 2014; Li et al., 2018; Raesi and Maddahian, 2022).

For the problem of hydrocyclone underflow entrainment, many scholars have carried out a lot of research on the structural parameters and operating parameters of the hydrocyclone. Dueck et al. (2010) studied the water-injection hydrocyclone and established the mathematical model of the water-injection rate and water-injection position on the grading particle size and grading efficiency. The study showed that water injection can improve the classification efficiency of hydrocyclone and have the effect of

online adjustment. Dian et al. (2024) found that 90° angle spiral inlet hydrocyclone has better flow field stability. The simulation comparison verified that this structure can effectively reduce the misalignment of the coarse and fine particles. Banerjee et al. (2024) found that the Cavex® double effect (DE) hydrocyclone can effectively reduce the fine particles in the underflow. Dou et al. (2020) established a PSO-SVM model and analyzed the trend of industrial injection hydrocyclone classification efficiency with parameters by training dataset, which showed that the highest efficiency was achieved when the diameter of the underflow opening was 50 mm, the inlet pressure was 0.25 MPa, and the injection pressure was 0.04 MPa. Ye et al. (2019) found that a conical section with a modified cone can help to improve the separation accuracy and separation efficiency of hydrocyclones. Ji et al. (2019) found that the laminar spiral inlet structure consumes less energy and mitigates the misplacement of the coarse and fine particles in the overflow and underflow. Dian et al. (2023) proposed a conical inlet hydrocyclone, and through numerical simulation and comparison with the basic hydrocyclone, this structure can effectively reduce the effect of particle misalignment. Zhang et al. (2022) proposed a spiral inlet structure hydrocyclone and used numerical simulation to compare it with the traditional tangential inlet hydrocyclone, and the results showed that the spiral inlet hydrocyclone has a more stable flow field and higher separation accuracy. Li et al. (2021) carried out a numerical simulation study on the height-to-width ratio of the rectangular inlet of the hydrocyclone and obtained the influence laws of the height-to-width ratio of the rectangular inlet on the pressure field, velocity field, air column, turbulence intensity, and separation efficiency. Zhao et al. (2021) proposed a multi-channel feed inlet based on the Archimedean helix and used numerical simulation to comparatively study the hydrocyclone with conventional tangential and new helix feed inlets. The results showed that the structure has superior classification performance than the conventional design. Hou et al. (2021) used numerical simulations to analyze the flow field characteristics, separation efficiency, and spatial distribution of particles in a flat-bottomed hydrocyclone and found that the wide flat-bottomed structure increases the separation particle size and reduces the underflow entrainment. Jiang et al. (2019, 2020) found that a flat-bottomed hydrocyclone with a cone angle close to 180° is more suitable for separating non-uniform slurries containing a high concentration of coarse particles and based on this, a W-type hydrocyclone was proposed, which can effectively alleviate the underflow entrainment of fines. Hwang et al. (2012) installed a conical top plate for a 20 mm hydrocyclone can effectively reduce the low-velocity zone near the surface of the outer swirl, reduce the circulation, and improve the particle separation efficiency.

Numerical simulations using Computational Fluid Dynamics (CFD) techniques have been widely used (Jing et al., 2021; Zhang and Tao, 2023; Wang et al., 2016). However, making accurate flow field predictions requires the selection of appropriate turbulence models and multiphase flow models, and the main turbulence models applied in hydrocyclones are the RSM model and the LES model (Dehdarinejad and Bayareh, 2022; Dehdarinejad et al., 2022; Dehdarinejad and Bayareh, 2023a). Multiphase flow models include the VOF model, the Mixture model, and the Euler model. The VOF model is widely used to study the distribution of gas-liquid two-phase flow in hydrocyclones. In recent years, the Mixture and Euler models have successfully predicted the particle motion in hydrocyclones (Xiong et al., 2023; Zhang et al., 2017; Wang et al., 2009). Wang et al. (2024) used Computational Fluid Dynamics (CFD) and Particle Image Velocimetry (PIV) techniques to simulate the flow field of a hydrocyclone and used a refractive index matching method to improve the accuracy of PIV measurements. Vakamalla and Mangadoddy (2019) explored the development of a 250 mm hydrocyclone air column and particle distribution using the Mixture model and LES model and verified the flow field by Laser Doppler Velocimetry and the predicted particle distribution curves were in good agreement with the experimental data. Kharoua et al., (2010) used different turbulence models to simulate a hydrocyclone and they both found that the RSM simulations were closest to the experimental results. Padhi et al. (2019) used RSM, VOF, and Mixture models to predict the hydrocyclone separation process and explore the effect of vortex finder and feed parameters on short-circuit flow and classification efficiency. Zheng et al. (2024) used a Reynolds stress model to obtain the turbulent flow characteristics within the ECSF and a discrete phase model to predict the particle trajectories to derive the separation performance. The accuracy of the simulation model has been verified experimentally. Dehdarinejad (2023b) conducted numerical simulations using the Reynolds stress method (RSM) and Eulerian-Lagrangian scheme to predict the collection grade efficiency, the

Euler number (Eu), and the cut-off size diameter for various combinations of the performance objectives of the cyclone.

However, there were fewer industrial experimental studies of the water-injection hydrocyclone, with most of the related research being numerical simulations and theoretical studies. Therefore, this paper proposed to alleviate the problem of underflow entrainment by adding a water-injection structure in the cone segment near the apex. Appropriate water injection could loosen and classify the settled particles on the wall of the conical section area, alleviate the underflow entrainment and improve the classification effect. Its working principle is shown in Fig. 1. In this paper, numerical simulation was used to study the water-injection hydrocyclone and conventional hydrocyclone to discuss the feasibility of the water-injection hydrocyclone. Then, industrial tests were conducted to investigate the effect of water-injection flow rate on the content of $-74 \mu\text{m}$ particles in the underflow and the classification efficiency.

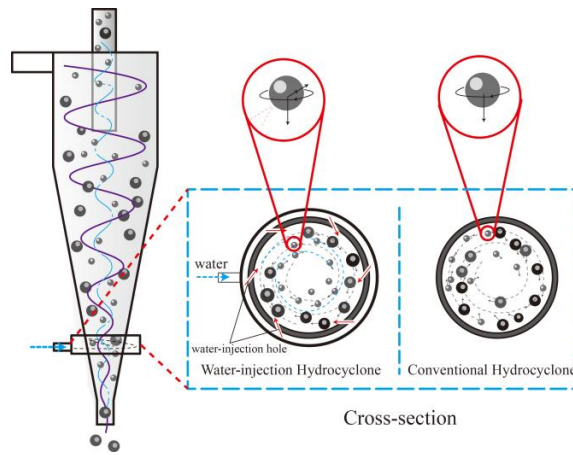


Fig. 1. Schematic diagram of water-injection hydrocyclone

2. Research Methodology

2.1. Simulation study

2.1.1. Geometry

The structural parameters of the hydrocyclone are shown in Fig. 2(a) and Table 1. The difference between the water-injection hydrocyclone and the conventional hydrocyclone lies in the additional water-injection structure in the cone section. The diameter of the water-injection hole was 1 mm. The structure of the water-injection hydrocyclone was modeled using the three-dimensional software SOLIDWORKS2021, with the center above the feed body as the coordinate origin and the direction of the underflow opening as the positive direction of the Z-axis, as shown in Fig. 2(b). To facilitate the analysis, several characteristic sections were chosen, including the axis center section ($Y = 0$), the cross-section at the cone section ($Z_1 = -400 \text{ mm}$), and the cross-section at the column section ($Z_2 = -200 \text{ mm}$), as shown in Fig. 2.

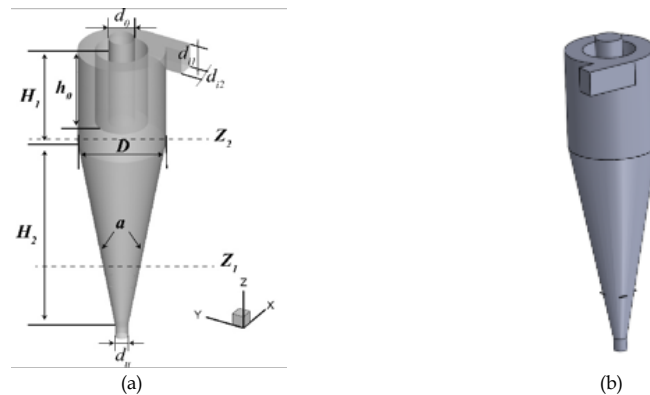


Fig. 2. Hydrocyclone simulation geometry model

Table 1. Structural parameters of hydrocyclone

Structure parameters	Size
Body diameter D /mm	200
Height of cylinder section H_1 /mm	240
Height of cone section H_2 /mm	480
Size of inlet $d_{i1} \times d_{i2}$ /mm	60×40
Overflow pipe diameter d_o /mm	60
Overflow pipe insertion depth h_o /mm	188
Apex diameter d_u /mm	30
cone angle $\alpha/^\circ$	20

The ICEM CFD software was used to mesh the fluid domain of the water-injection hydrocyclone. As shown in Fig. 3, the hexahedral structured mesh was chosen over the tetrahedral unstructured mesh due to its benefits of shorter computation time, faster convergence speed, and smaller discretization error.

The number of grids had an impact on the model prediction results; too few grids will affect the calculation accuracy and too many grids will prolong the simulation calculation time. Therefore, the number of grids should be controlled within a suitable range under the condition of maintaining computational accuracy. The grid number of hydrocyclone was divided into 163k, 224k, 270k, 310k, and 351k, and the tangential velocity value at the axial height $Z=-200\text{mm}$ was chosen as the basis of grid independence verification. As seen in Fig. 4, the tangential velocity of the hydrocyclone remained constant after the number of grids was greater than 270k. Therefore, the grid number of 270k was determined.

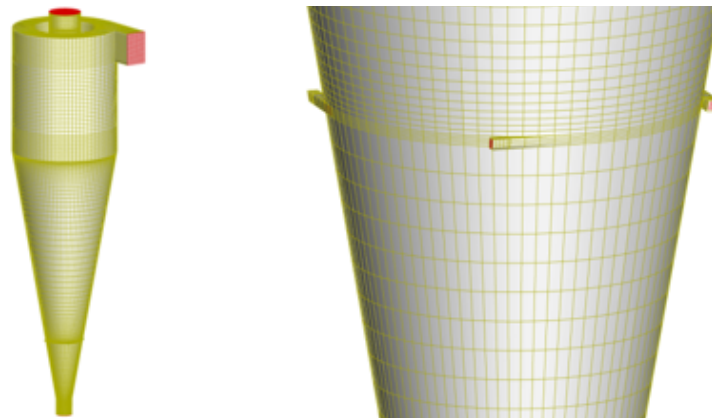


Fig. 3. Grid division

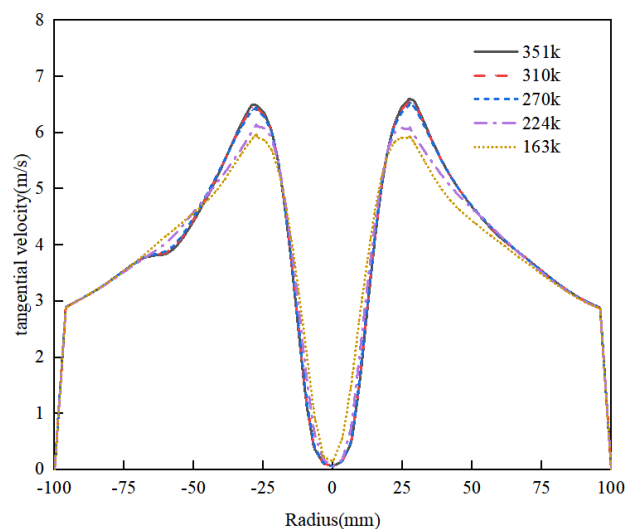


Fig. 4. Number of grids

2.1.2. Model description

The fluid motion state inside the hydrocyclone is mainly a strong rotational shear flow formed by internal swirl flow, external swirl flow and air column. Numerical simulation is the main means to study such complex turbulent flow. The fluid motion state inside the hydrocyclone is mainly a strong rotational shear flow formed by internal swirl flow, external swirl flow and air column. Numerical simulation is the main means to study such complex turbulent flow. The RSM turbulence model accurately predicts the Reynolds stress and anisotropy of the complex flow field. Due to the fast flow velocity and high turbulence intensity in the internal flow field of the hydrocyclone, the RSM model is often used in the numerical simulation of the hydrocyclone.

(1) RSM turbulence model control equations:

- Control equations:

$$\frac{\partial}{\partial t}(\rho \overline{u_i' u_j'}) + \frac{\partial}{\partial x_k}(\rho \overline{u_i' u_j' u_k'}) = D_{T,ij} + D_{L,ij} + P_{ij} + G_{ij} + \Phi_{ij} + \varepsilon_{ij} + F_{ij} \quad (1)$$

- Among them, Turbulent kinetic energy diffusion term:

$$D_{T,ij} = -\frac{\partial}{\partial x_k}(\rho \overline{u_i' u_j' u_k'} + \overline{p' u_i'} \delta_{kj} + \overline{p' u_j'} \delta_{ik}) \quad (2)$$

- Molecular viscosity diffusion term:

$$D_{L,ij} = -\frac{\partial}{\partial x_k} \left[\mu \frac{\partial}{\partial x_k} (\overline{u_i' u_j'}) \right] \quad (3)$$

- Shear stress generation term:

$$P_{ij} = \rho \left(\overline{u_i' u_k'} \frac{\partial u_j}{\partial x_k} + \overline{u_j' u_k'} \frac{\partial u_i}{\partial x_k} \right) \quad (4)$$

- Buoyancy generation term:

$$G_{ij} = -\rho \beta (g_i \overline{u_j' \theta} + g_j \overline{u_i' \theta}) \quad (5)$$

- Pressure strain term:

$$\Phi_{ij} = p' \left(\frac{\partial u_i}{\partial x_j} + \frac{\partial u_j}{\partial x_i} \right) \quad (6)$$

- Viscous dissipative term:

$$\varepsilon_{ij} = p' \frac{\partial u_i}{\partial x_k} \frac{\partial u_j}{\partial x_k} \quad (7)$$

- Fluid rotation generation term:

$$F = -2\rho \Omega_k (\overline{u_j' u_m'} e_{ikm} + \overline{u_i' u_j'} e_{ikm}) \quad (8)$$

(2) Euler model:

The Euler model, also known as the two-fluid model, solves the momentum and continuity equations for each phase, and the coupling is realized by the pressure term and the exchange coefficients at the interfaces of each phase, which can obtain higher accuracy than the Mixture model when the drag law between the phases is known.

- Euler model mass equation:

$$(\alpha_t \rho_t) + \nabla \cdot (\alpha_t \rho_t v_t) = 0 \quad (9)$$

- The Momentum Equation for the solid-liquid phase is respectively:

$$\frac{\partial}{\partial t}(\alpha_f \rho_f v_f) + \nabla \cdot (\alpha_f \rho_f v_f v_f) = -\alpha_f \nabla P + \nabla \cdot \bar{\tau}_f + \alpha_f \rho_f g + K_{sf}(v_s - v_f) \quad (10)$$

$$\frac{\partial}{\partial t}(\alpha_s \rho_s v_s) + \nabla \cdot (\alpha_s \rho_s v_s v_s) = -\alpha_s \nabla P - \nabla P_s + \nabla \cdot \bar{\tau}_s + \alpha_s \rho_s g + K_{sf}(v_f - v_s) \quad (11)$$

where v_f and v_s are the average flow velocity of the solid-liquid two-phase. P is the pressure shared by the solid-liquid two-phase. The stress tensor of the solid-liquid two-phase is $\bar{\tau}_f$ and $\bar{\tau}_s$.

2.1.3. Simulation conditions

The Euler model and RSM model were selected to simulate the multiphase flow field inside the water-injection hydrocyclone. There were two types of inlets in the water-injection hydrocyclone, including the feed inlet and the water-injection hole. The inlet boundary was set to "Velocity-inlet" and the value of velocity was 3 m/s. From the calculation, the volume fraction of solid phase particles was 16.86%. the boundary conditions of the underflow and overflow ports were set to "pressure outlet", the air phase return volume fraction was set to 1, and the boundary condition of the hydrocyclone wall was

“No Slip”. Quartz sand was selected as the material, and the particle phase was set as inertial collision particles with a density of 2630 kg/m³. Seven different particle sizes were selected, and the particle size distributions are shown in Table 2. The QUICK format was used for the discrete format, the pressure-velocity coupling was PRESTO! and the SIMPLE algorithm.

Table 2. Particle size distribution

Mean size/ μm	Yield /%	Volume fraction /%
10	18.98	3.2
29	23.13	3.9
41	11.86	2
59	21.71	3.66
89	8.90	1.5
129	8.90	1.5
150	6.52	1.1

2.2. Experimental studies

Comparative tests on water-injection hydrocyclone and conventional hydrocyclone were carried out to clarify the difference between them in terms of the concentration of each product, particle size composition, underflow yield, and classification efficiency, thus determining the effectiveness of the water-injection structure in alleviating the phenomenon of underflow entrapment. Further, single-factor tests were also conducted.

2.2.1. Experimental program

To investigate the effect of water injection on the hydrocyclone separation performance, an industrial-scale hydrocyclone separation test platform was built, as shown in Fig. 5. During the test, the slurry was mixed in the barrel and pumped into the hydrocyclone. After separation, the overflow and underflow products were converged into the mixing barrel to form a closed loop to maintain the stability of the feed concentration. When the system was stabilized, the injection water valve was open. After the flow rate was stabilized, multiple sets of duplicate samples of feed, overflow, and underflow were taken for testing to reduce the error. Take concentration, underflow yield, underflow -74 μm particle size yield and comprehensive classification efficiency as the calculation and analysis index.

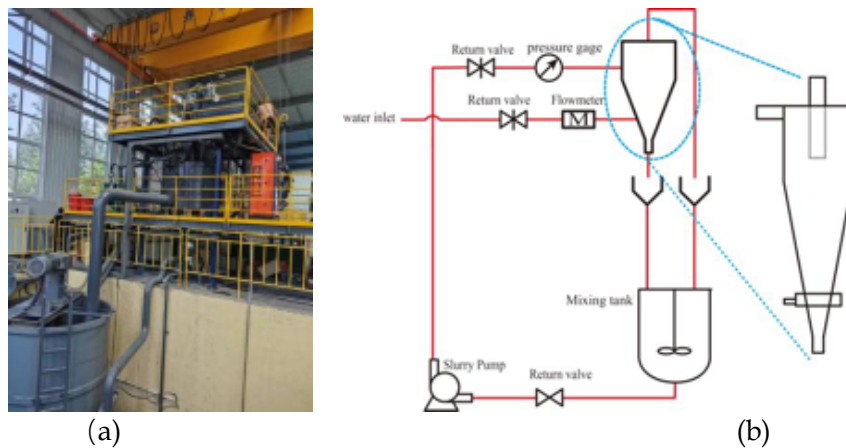


Fig. 5. Schematic diagram of the test system

Table 3 summarizes the structural parameters of the hydrocyclone in detail. Considering the actual working conditions, $\Phi 350\text{mm}$ hydrocyclone was selected for this test, as shown in Fig. 6. The selected iron ore materials were from a company in Liaoning, China. Table 4 summarizes its particle-size composition. From the data in Table 4, it could be seen that the content of -74 μm particles was 55.36%, the content of -100 μm particles was 64.32%, and the content of -154 μm particles was 77.56%. The experimental program was designed as follows. Firstly, the water-injection hydrocyclone and conventional hydrocyclone were compared under the feed pressure of 0.08MPa and feed concentration

of 27%. The water-injection flow rate was set as 0 m³/h, 1 m³/h, 2 m³/h, 3 m³/h, 4 m³/h, 5 m³/h (the proportion of the feed flow rate of 0%, 1%, 2%, 3%, 4%, 5%), respectively.



Fig. 6. Schematic diagram of water-injection hydrocyclone

Table 3. Structural parameters of hydrocyclone in the industrial test

Structure parameters	Size
Body diameter /mm	350
Height of cylinder section /mm	600
Size of inlet /mm	160
Overflow pipe diameter /mm	120
Apex diameter /mm	60
Overflow pipe insertion depth /mm	320
Cone angle /°	20

Table 4. Feed size distribution

Mesh number	Size/ μm	Content /%	Negative accumulation /%
-500	-30	34.25	34.25
+500~-325	30~45	5.53	39.78
+325~-200	45~74	15.58	55.36
+200~-150	74~100	8.96	64.32
+150~-100	100~154	13.24	77.56
+100~-60	154~300	15.53	93.09
+60	+300	6.91	100

3. Results and discussion

3.1. Simulation results and discussion

3.1.1. Pressure

The pressure field could reflect the treatment performance and energy loss of the hydrocyclone, which is a complex flow field composed of free vortices and solenoidal vortices. Fig. 7 and Fig. 8 show the static pressure distribution cloud and the curve comparison of the Z1 section, respectively. It is worth noting that the blank region in the center of the hydrocyclone is the air core region, defined as the region where the air volume fraction is greater than 90%, which is similar to all other clouds in this study. From the figure, it can be seen that the pressure generated inside the water-injection hydrocyclone is greater than that of the conventional hydrocyclone, and both of them have the same pressure distribution law, which is gradually reduced from the outer wall of the hydrocyclone to the centerline, and is centrosymmetric. The pressure near the inner wall of the water-injection hydrocyclone is higher than that of the conventional hydrocyclone because water injection will bring higher pressure driving force to the outer swirl, which is conducive to the fine particles leaving the outer swirl and entering the inner swirl, thus better separating the materials. Fig. 9 presents the air core distribution cloud and air core

and comparison of air column. As shown in the Fig. 9(b), compared with the conventional hydrocyclone, the air core of the water-injection hydrocyclone has a smaller variation amplitude, and its internal flow field is more stable, which provides stable conditions for material separation.

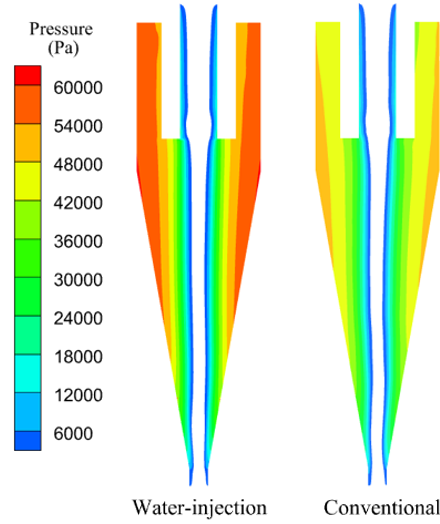


Fig. 7. Pressure comparison cloud diagram

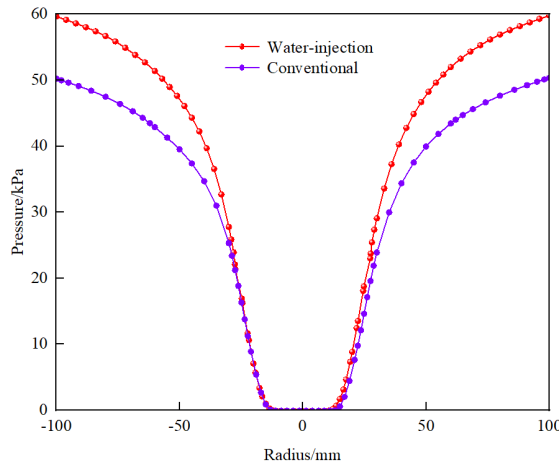
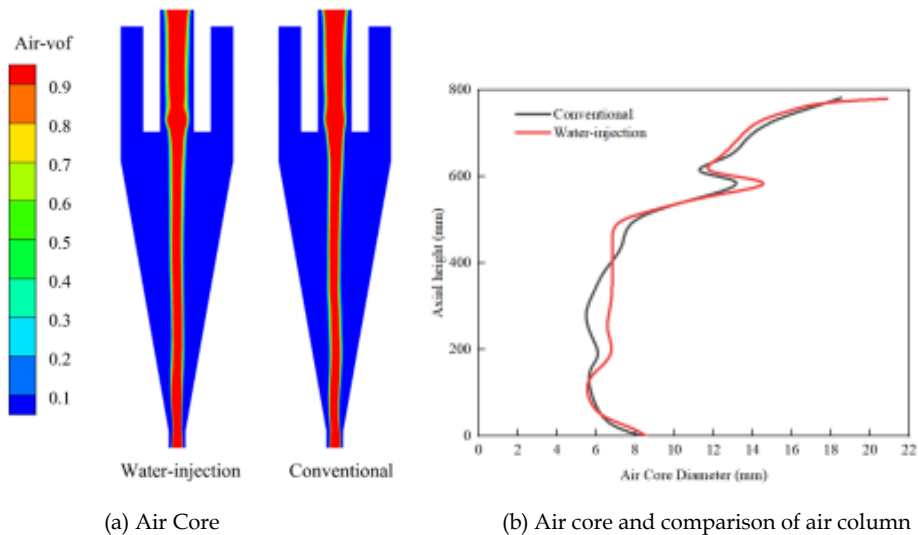


Fig. 8. Comparison of radial pressure distribution in the Z_1 section



(a) Air Core

(b) Air core and comparison of air column

Fig. 9. Air core and Comparison of air column diameters

3.1.2. Tangential velocity

Fig. 10 shows the cloud diagram of the tangential velocity distribution of two kinds of hydrocyclones. Fig. 11 displays the distribution curves at different cross-section positions. The magnitude of the tangential velocity directly determines the strength of the centrifugal force field inside the hydrocyclone, therefore it is of great significance to study the tangential velocity. From the figure, it can be seen that the water injection did not affect the change rule of tangential velocity, “M” distribution. Both from the wall to the center of the hydrocyclone, the tangential velocity first increases and then decreases, the maximum value appears in the junction of the forced vortex and the free vortex. With the decrease of the radial distance, the tangential velocity decreases rapidly, and in the center of the hydrocyclone, it falls to zero. At the Z2 position, the velocity change gradient of the tangential velocity of the water-injection hydrocyclone is more obvious and the classification effect is better compared with that of the conventional hydrocyclone. This is because water injection can provide an additional thrust to increase the tangential velocity, which also means that water injection can increase the centrifugal force field and therefore improve the separation performance of the hydrocyclone.

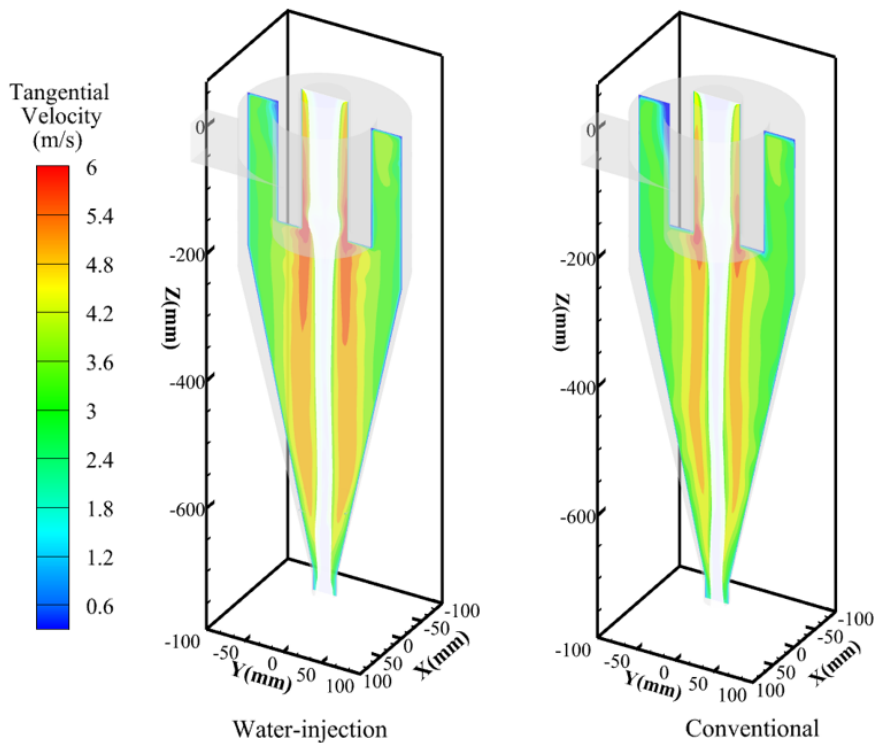


Fig. 10. Contours of the tangential velocity distributions

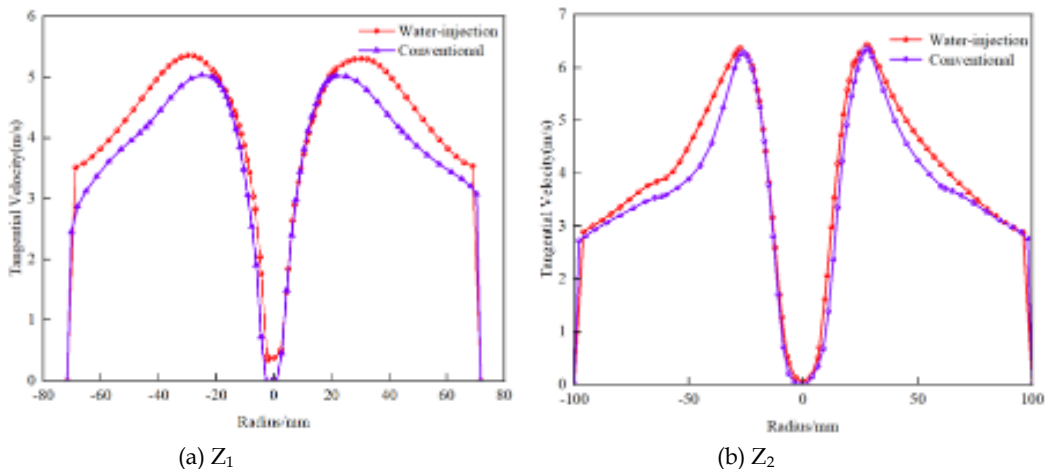


Fig. 11. Comparison of the tangential velocity distributions

3.1.3. Axial velocity

Fig. 12 and Fig. 13 show the axial velocity cloud diagram and the axial velocity distribution curves at different cross sections for the two hydrocyclones, respectively. The magnitude of the axial velocity directly determines the residence time of the material in the hydrocyclone, so the axial velocity affects the separation accuracy of the hydrocyclone. As can be seen from the figure, the axial velocity of the two types of hydrocyclone shows a symmetrical distribution. Along the radial position, from the wall to the center, it first decreases and then increases, and the main separation area axial velocity maximum value appears in the center of the axis. The maximum value of the overflow outlet area appeared in the radius of about 15mm, and the axial velocity extreme value of the water-injection hydrocyclone is higher than that of the conventional hydrocyclone. At the Z1 position, the axial velocity of both hydrocyclones is the same, but near the center axis, the axial velocity of the water-injection hydrocyclone is slightly larger than that of the conventional hydrocyclone. It can be illustrated that water injection slightly increases the motion velocity of the outer swirl and also increases the motion velocity of the inner swirl, resulting in a more stable flow field and better separation performance in this region.

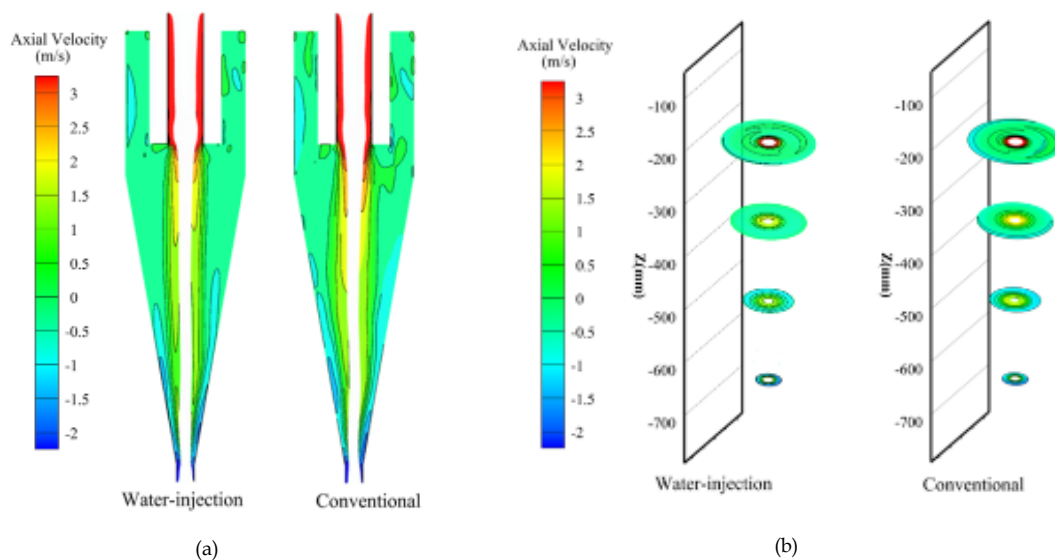


Fig. 12. Contours of the axial velocity distributions

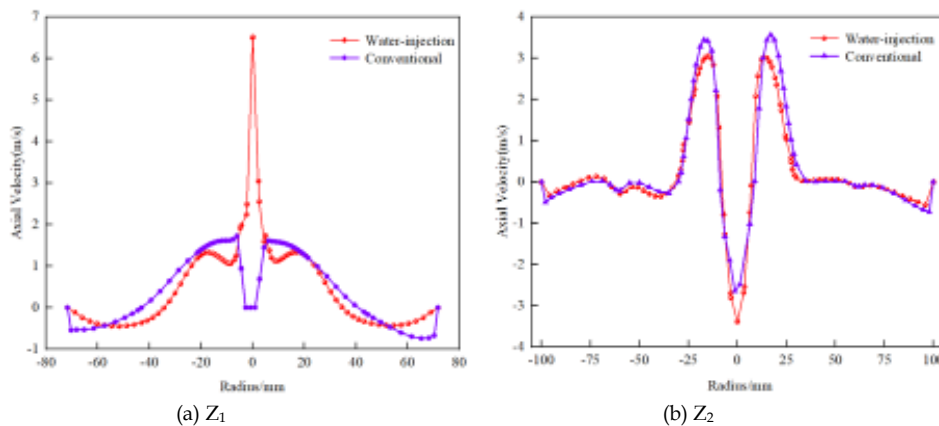


Fig. 13. Comparison of the axial velocity distributions.

3.1.4. Turbulence intensity

The turbulence intensity shows the degree of turbulence in the internal flow field. The distribution of turbulence intensity of the two hydrocyclones is shown in Fig. 14. From the figure, it can be seen that the turbulence intensity of the conventional hydrocyclone is higher at the lower part of conical section, indicating that the flow field near the underflow is relatively turbulent. This region of intense turbulence

makes it easier for fine particles to be carried into the underflow by the outer swirl flow, resulting in the problem of fines entrapment in the underflow. Compared with conventional hydrocyclone, water injection can alleviate the turbulence intensity and make the flow field more stable, thus alleviating the influence to fine particles and improving the separation performance of the hydrocyclone.

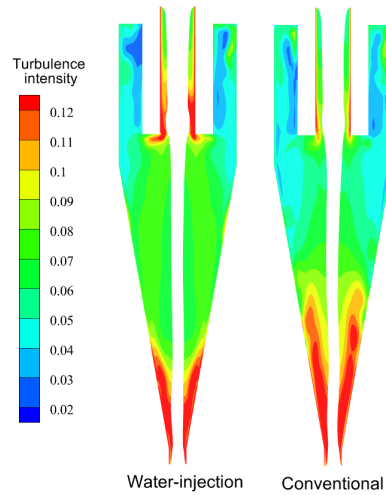


Fig. 14. Contours of the turbulent intensity distributions

3.1.5. Particle volume fraction

The movement of particles is mainly affected by centrifugal force. The larger the particle size the greater the centrifugal force, and the more it moves outward. Two different particle sizes of $29\ \mu\text{m}$ and $129\ \mu\text{m}$ were selected to analyze the distribution of particles in the two kinds of hydrocyclones. Fig. 15(a) shows the cloud diagram of the distribution of $29\ \mu\text{m}$ particles inside the two kinds of hydrocyclones. From Fig. 15(a), it can be seen that compared with the conventional hydrocyclone, the fine particles in the water-injection hydrocyclone are more likely to enter the inner swirl flow and be discharged from the vortex finder. This results in a decrease in particle content at locations below the water-injection structure and a reduction in the number of fine particles in the underflow product. Fig. 15(b) shows the distribution cloud of particles with $129\ \mu\text{m}$ particle size in the two hydrocyclones. From the figure, it can be seen that the water injection can disperse the coarse particles settled on the wall surface of the cone section. Therefore, the coarse particles are reduced obviously in the upper part of the cone section, while increased below the water injection position resulting in more of them to discharge from the underflow pipe. The elevated content of coarse particles in the underflow product, combined with the reduction of fine particles in the underflow, improves the classification accuracy of the hydrocyclone.

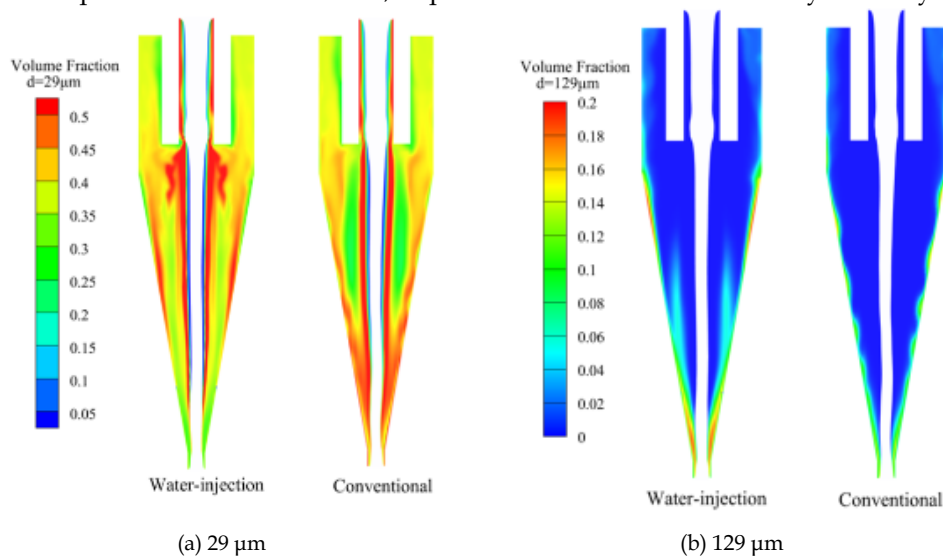


Fig. 15. Contours of particle volume fraction distributions

3.2. Experimental results and discussion

Fig. 16 shows the effect of the water-injection flow rate on the hydrocyclone product concentration. Compared to the conventional hydrocyclone, the underflow concentration and overflow concentration decrease after water injection. The water-injection flow rate is negatively correlated with the underflow concentration and overflow concentration. Increasing the water-injection flow rate from 0 m³/h to 5 m³/h reduces the underflow concentration from 82.63% to 81.13% and the overflow concentration from 10.97% to 10.03%. Since the injection flow rate is much smaller in value compared to the treatment capacity, the impact on the overflow and underflow concentrations is also relatively small. Fig. 17 displays the effect of the water-injection flow rate on the hydrocyclone underflow yield. From Fig. 17, it can be seen that the water-injection flow rate is positively correlated with the underflow yield. As the water-injection flow rate increases from 0m³/h to 5m³/h, the underflow yield increases from 68.46% to 71.72%. This is because with the increase of water-injection flow rate, the water flow will disperse the particles deposited in the cone section, and the particles re-enter the swirl for grading and then discharge from the overflow port. However, the increase in the water-injection flow rate causes an increase in water volume in the hydrocyclone, which will dilute the products of all levels to different degrees and reduce the concentration.

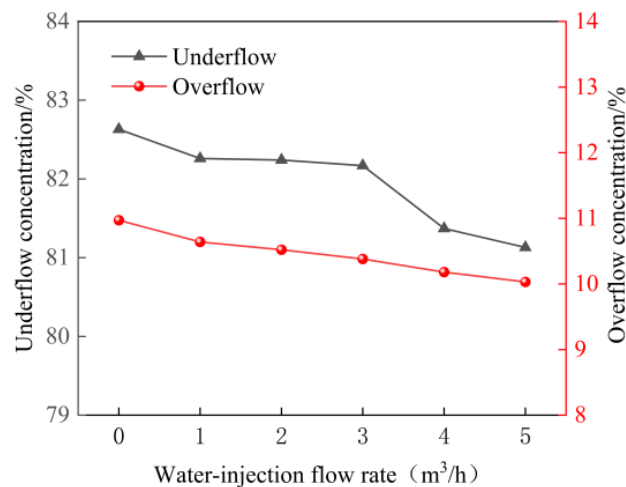


Fig.16. Effect of water-injection flow rate on hydrocyclone product concentration

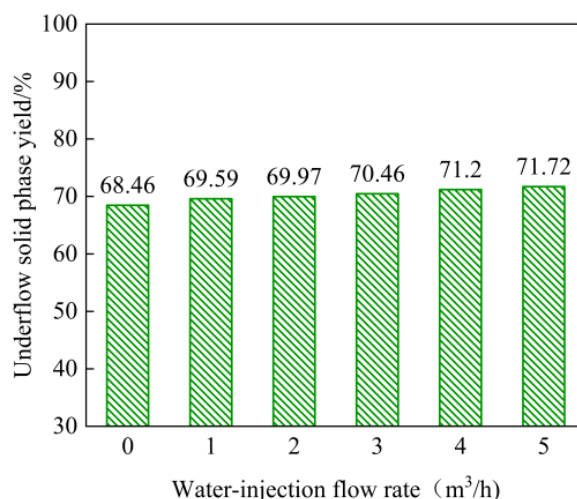


Fig. 17. Effect of water-injection flow rate on the underflow solid phase yield

Fig. 18 shows the variation of -74 μ m particle content in overflow and underflow with water-injection flow rate. Compared with the conventional hydrocyclone, the -74 μ m particle content in the underflow of the water-injection hydrocyclone decreases from 26.34% to 23.95%, and it increases from 97.03% to 97.79% in the overflow when the water-injection flow rate varies from 0 to 4 m³/h. If the water-injection

flow rate is increased more, the $-74\ \mu\text{m}$ particle content in the underflow increases and decreases in the overflow. This is because that, with the increase of injection flow rate, the water flow will entrain fine particles across the locus of zero vertical velocity into the internal swirl, which will be discharged by the overflow. This leads to a decrease in the $-74\ \mu\text{m}$ particle content in the underflow and an increase in the $-74\ \mu\text{m}$ particle content in the overflow. When the injection flow rate is too large, some coarse particles are entrained by the water flow to enter the inner swirl, increasing the percentage of $-74\ \mu\text{m}$ particle size in the underflow, which in turn reduces the separation accuracy.

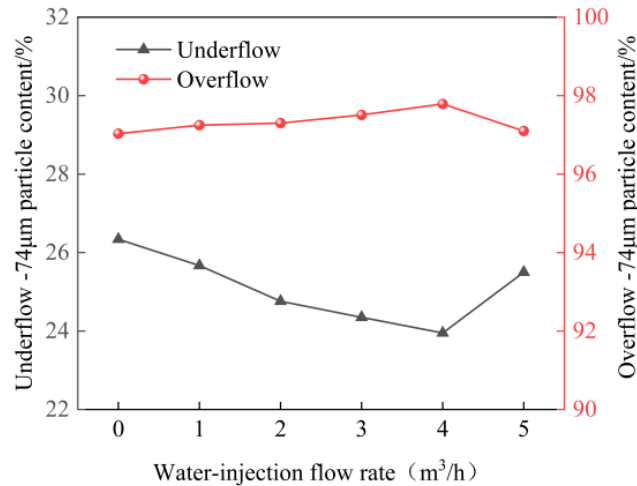


Fig. 18. Effect of water-injection flow rate on the hydrocyclone product $-74\ \mu\text{m}$ particle content

The effect of water-injection flow rate on the classification performance was explored by taking the comprehensive classification efficiency of $-74\ \mu\text{m}$ particles as an evaluation index. As can be seen from Fig. 19, compared with the conventional hydrocyclone, the integrated classification efficiency of $-74\ \mu\text{m}$ particles increased from 69.22% to 73.03% after adding the water-injection structure. With the increase of water-injection flow rate from 1 m³/h to 5 m³/h, the integrated classification efficiency of $-74\ \mu\text{m}$ particles of the water-injection hydrocyclone shows a trend of first increase and then decrease, and the integrated classification efficiency of $-74\ \mu\text{m}$ particles of the hydrocyclone reaches the maximum value of 73.03% when the water-injection flow rate is 4 m³/h. When the number of water-injection holes is unchanged, adjusting the water-injection flow rate within an appropriate range can alleviate the problem of fines entrapment in the underflow and improve the comprehensive grading efficiency. In other words, the experimental results confirm that the content of $-74\ \mu\text{m}$ particles in the underflow can be reduced and the comprehensive classification efficiency can be improved under suitable condition of injection water flow rate, which is also consistent with the conclusions drawn from the simulation results about the effect of water injection on the separation of fine particles.

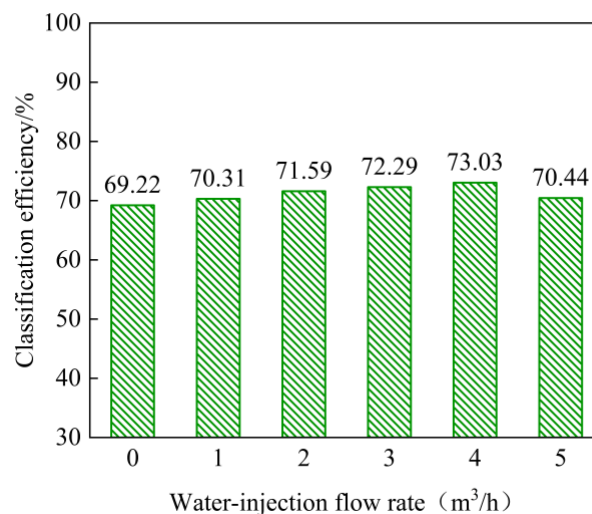


Fig. 19. Effect of water-injection flow rate on comprehensive classification efficiency

4. Conclusions

A water-injection hydrocyclone was proposed aiming to solve the problem of underflow entrapment fines in the process of metal ore separation by hydrocyclone, and numerical simulation and experimental study were carried out. Accordingly, the following main conclusions are made.

Compared with the conventional hydrocyclone, the static pressure of the water-injection hydrocyclone is larger, the turbulence intensity is smaller, and the internal flow field is more stable. The tangential velocity and axial velocity are higher, which is more conducive to improving the separation accuracy.

With the increase of water-injection flow, the comprehensive classification efficiency shows the trend of increasing first and then decreasing, when the water-injection flow is 4 m³/h, the content of underflow stream -74 μm particles reaches the minimum value of 23.95%, and the comprehensive classification efficiency reaches the maximum value of 73.03%.

Compared with the conventional hydrocyclone, the water-injection hydrocyclone underflow -74 μm particle content was reduced from 26.34% to 23.95%, and the classification efficiency was increased from 69.22% to 73.03%. which improved the underflow entrapment fine.

Acknowledgments

Funding: This research was funded by the LiaoNing Revitalization Talents Program, China (XLYC2204015)

References

- BANERJEE, C.; CEPEDA, E.; SWITZER, D.; HUNTER, S. 2024. *Application Potential of Cavex® Double Effect Hydrocyclone for the Classification of Mine Tailings - A Pilot Scale Study*. Mineral Processing and Extractive Metallurgy Review, doi:10.1080/08827508.2023.2298376
- DEHDARINEJAD, E., BAYAREH, M. 2021. *An Overview of Numerical Simulations on Gas-Solid Cyclone Separators with Tangential Inlet*. ChemBioEng Reviews, 8(4), 375-391.
- DEHDARINEJAD, E., BAYAREH, M. 2022. *Performance improvement of a cyclone separator using spiral guide vanes with variable pitch length*. Journal of the Brazilian Society of Mechanical Sciences and Engineering, 44(11).
- DEHDARINEJAD, E., BAYAREH, M., ASHRAFIZAADEH, M. 2022. *Impact of cone wall roughness on turbulence swirling flow in a cyclone separator*. Chemical Papers, 76(9), 5579-5599.
- DEHDARINEJAD, E., BAYAREH, M. 2023a. *Experimental and numerical investigation on the performance of a gas-solid cyclone with twisted baffles and roughened cone surface*. Powder Technology, 420.
- DEHDARINEJAD, E., BAYAREH, M. 2023b. *Performance analysis of a novel cyclone separator using RBFNN and MOPSO algorithms*. Powder Technology, 426.
- DIAN, Y.E., FAN, H.H., SU, Z.F., X, G.T., ZOU, R.P., YU, A.B., Kuang, S.B. 2023. *Numerical study of the multiphase flows and separation performance of hydrocyclone with tapered cross-section inlet*. Powder Technology, 416, doi:10.1016/j.powtec.2022.118208
- DIAN, Y.E., X, G.T., FAN, H.H., CUI, J.X., TAN, C., ZHANG, Y.H., ZOU, R.P., KUANG, S.B., YU, A.B. 2024. *Numerical investigation of hydrocyclone inlet configurations for improving separation performance*. Powder Technology, 434.
- DOU, D.Y., QIU, Z.Y., YANG, J.G. 2020. *Parameter optimization of an industrial water-injection hydrocyclone in the Taixi coal preparation plant*. International Journal of Coal Preparation and Utilization, 42(8): 2357-2365.
- DUECK, J., PIKUSHCHAK, E., MINKOV, L., FARGHALY, M., NEESSE, T. 2010. *Mechanism of hydrocyclone separation with water-injection*. Minerals Engineering, 23(4), 289-294.
- GHODRAT, M., KUANG, S. B., YU, A. B., VINCE, A., BARNETT, G. D., BARNETT, P. J. 2014. *Numerical analysis of hydrocyclones with different conical section designs*. Minerals Engineering, 62, 74-84.
- HWANG, K.-J., HWANG, Y.-W., YOSHIDA, H., SHIGEMORI, K. 2012. *Improvement of particle separation efficiency by installing conical top-plate in hydrocyclone*. Powder Technology, 232, 41-48.
- HOU, D., CUI, B., ZHANG, H., ZHAO, Q., JI, A., WEI, D., FENG, Y. 2021. *Designing the hydrocyclone with flat bottom structure for weakening bypass effect*. Powder Technology, 394, 724-734.
- JI, L., KUANG, S.B., YU, A.B. 2019. *Numerical investigation of hydrocyclone feed inlet configurations for mitigating particle misplacement*. Industrial & Engineering Chemistry Research. 58, 16823-16833.

- JIANG, L.Y., LIU, P.K., ZHANG, Y.K., YANG, X.H., WANG, H., GUI, X.H. 2019. *Design boundary layer structure for improving the particle separation performance of a hydrocyclone*, Powder Technol. 350 1–14.
- JIANG, L.Y., LIU, P.K., YANG, X.H., ZHANG, Y.K., LI, X.Y., ZHANG, Y.L., WANG, H. 2020. *Experimental research on the separation performance of W-shaped hydrocyclone*. Powder Technology. DOI:10.1016/j.powtec.2020.06.047
- JING, J.Q., ZHANG, S.J., TAN, J.T. 2021. *Numerical simulation study of offshore heavy oil desanding by hydrocyclones*. Separation and Purification Technology, 258: 118051.
- KHAROUA, N., KHEZZAR, L., NEMOUCHI, Z. 2010. *Computational fluid dynamics study of the parameters affecting oil – water hydrocyclone performance*. Proceedings of the Institution of Mechanical Engineers, Part E: Journal of Process Mechanical Engineering, 224(2), 119–128.
- LI, C.X., BAI, Y., DONG, Q.G., LIU, G.Q., ZHAO, J.Y. 2018. *Application of a small cone hydrocyclone on high ash fine coal pre-desliming flotation*. International Journal of Coal Preparation and Utilization, 39(5), 233–235.
- LI, F., LIU, P.K., YANG, X.H., ZHANG, Y.K., JIANG, L.Y., WANG, H. 2021. *The effects of the height-to-width ratio of the rectangular inlet on the flow field and separation performance by hydrocyclone*. International Journal of Coal Preparation and Utilization, 42(10): 3137-3154.
- MOGNON, J. L., DA SILVA, J. M., BICALHO, I. C., ATAÍDE, C. H., DUARTE, C. R. 2015. *Modular mini-hydrocyclone desilter type of 30mm: An experimental and optimization study*. Journal of Petroleum Science and Engineering, 129, 145–152.
- PADHI, M.; MANGADODDY, N.; SREENIVAS, T.; VAKAMALLA, T.R.; MAINZA, A.N. *Study on multi-component particle behaviour in a hydrocyclone classifier using experimental and computational fluid dynamics techniques*. Separation and Purification Technology, 2019, 229: 115698.
- RAESI, R., MADDAHIAN, R. 2022. *Numerical investigation of air-injected deoiling hydrocyclones using population balance model*. Chemical Engineering Science, 248, 117103.
- WANG, C.Z., CHEN, J.Z., SHEN, L., GE, L.H., 2019. *Study of flow behaviour in a three products hydrocyclone screen: numerical simulation and experimental validation*. Physicochemical Problems of Mineral Processing, 55(4), 879–895.
- WANG, L.Y., ZHENG, Z.C., WU, Y.X., GUO, J., ZHANG, J., TANG, C. 2009. *Numerical and experimental study on liquid-solid flow in a hydrocyclone*. Journal of Hydrodynamics, Ser. B, 21(3), 408–414.
- WANG, J.G., ZHENG, Y., WANG, H.L., BAI, Z.S., QIU, Y. 2024. *Investigation of the asymmetric flow structure in a hydrocyclone*. Asia-Pacific Journal of Chemical Engineering, doi:10.1002/apj.3080
- WANG, C.Y., YANG, Q., XU, X., WANG, H.L. 2016. *Computational Fluid Dynamics Simulation of the Impact of Structure on the Degassing Efficiency of a Cyclone*. Chemical Engineering & Technology, 39(3), 522–528.
- VAKAMALLA, T.R.; MANGADODDY, N. 2019. *The dynamic behaviour of a large-scale 250-mm hydrocyclone: A CFD study*. Asia-Pacific Journal of Chemical Engineering, 14(2): e2287.
- XIONG, Z.P., XU, J., LIU, C.J. 2023. *Interaction effects of inlet velocity and apex diameter on the separation performance of two-stage cone hydrocyclones*. Powder Technology, 422.
- YE, J.X., XU, Y.X., SONG, X.F., YU, J.G. 2019. *Novel conical section design for ultra-fine particles classification by a hydrocyclone*. Chemical Engineering Research and Design, 144, 135–149.
- ZHANG, L., YANG, L., HOU, H.C., ZHAO, Y.; LIN, J., ZHANG, Z.L., BU, C.Y., ZHENG, X.R., FU, D. 2023. *Experimental study of quartz classification in the enhanced gravity field using Falcon concentrator*. Physicochemical Problems of Mineral Processing, 59(6), doi:10.37190/ppmp/175242.
- ZHANG, Y.K., DUAN, Y.X., JIANG, L.Y., CAO, J.Z. 2022. *Classification performance of a novel hydraulic classifier equipped with a W-Shaped reflector*. Separations, 9(8): 212.
- ZHANG, X.B., TAO, Y.J. 2023. *CFD simulation on internal flow field of typical hydrocyclone for coal and development of novel hydrocyclone*. Particulate Science and Technology, 42(3), 469–481.
- ZHANG, C.E., WEI, D.Z., CUI, B.Y., LI, T.S., LUO, N. 2017. *Effects of curvature radius on separation behaviors of the hydrocyclone with a tangent-circle inlet*. Powder Technology, 305, 156–165.
- ZHENG, Y.B., SONG, T., NI, L. 2024. *Numerical simulation investigating the impact of regulated underflow rate on the performance of a cyclone with split flow*. Separation and Purification Technology, 345.
- ZHAO, Q., HOU, D.X., CUI, B.Y., WEI, D.Z., SONG, T., FENG, Y.Q. 2021. *Development of an integrated multichannel inlet for improved particle classification in hydrocyclones*. Advanced Powder Technology, 32(12): 4546–4561.